Fibroblasts and alectinib switch the evolutionary games that non-small cell lung cancer plays

Artem Kaznatcheev[1,2], Jeffrey Peacock[3], David Basanta[4], Andriy Marusyk[5], and Jacob G. Scott[2,6,7]

[1]Department of Computer Science, University of Oxford, Oxford, UK
[2]Department of Translational Hematology & Oncology Research, Cleveland Clinic, Cleveland, OH, USA
[3]Department of Radiation Oncology, Moffitt Cancer Center, Tampa, FL, USA
[4]Department of Integrated Mathematical Oncology, Moffitt Cancer Center, Tampa, FL, USA
[5]Department of Cancer Imaging and Metabolism, Moffitt Cancer Center, Tampa, FL, USA
[6]Department of Radiation Oncology, Cleveland Clinic, Cleveland, OH, USA
[7]Center for Proteomics & Bioinformatics, Case Western Reserve University School of Medicine, Cleveland, OH, USA

Heterogeneity in strategies for survival and propagation among the cells that constitute a tumour is a driving force behind the evolution of resistance to cancer treatment. The rules mapping the tumour's strategy distribution to the fitness of individual strategies can be represented as an evolutionary game. We develop a game assay to measure this property in co-culures of alectinib-sensitive and alectinib-resistant non-small cell lung cancer. The games are not only quantitatively different between different environments, but targeted therapy and cancer associated fibroblasts qualitatively switch the type of game being played from Leader to Deadlock. This provides the first empirical confirmation of a central theoretical postulate of evolutionary game theory in oncology: we can treat not just the player, but also the game. Although we concentrate on measuring games played by cancer cells, the measurement methodology we develop can be used to advance the study of games in other microscopic systems.

Tumors are heterogeneous, evolving ecosystems (*1*, *2*), composed of sub-populations of neoplastic cells that follow distinct strategies for survival and propagation (*3*). The success of a strategy defining any single neoplastic sub-population is dependent on the distribution of other strategies, and on various components of the tumour microenvironment, like cancer associated fibroblasts (CAFs) (*4*). The EML4-ALK fusion, found in approximately 5% of non-small cell lung cancer (NSCLC) patients, leads to constitutive activation of oncogenic tyrosine kinase activity of ALK, thereby "driving" the disease. Inhibitors of tyrosine kinase activity of ALK (ALK TKI) proved to be highly clinically efficacious, inducing tumor shrinkage and prolonging patient survival (*5*). Unfortunately, virtually all of the tumors that respond to ALK TKIs eventually relapse (*6*) which is an outcome typical of other oncogenic tyrosine kinases (*7*), and resistance to ALK TKI remains a major unresolved clinical challenge. Despite significant advances in deciphering molecular mechanisms of resistance (*8*), the evolutionary dynamics of ALK TKI resistance remains poorly understood. The inability of TKI therapies to completely eliminate tumor cells has been shown to be at least partially attributable to microenvironmental protection (*9*). CAFs are one of the main non-malignant components of tumor microenvironment and the interplay between them and tumor cells is a major contributor to microenvironmental resistance, including cytokine mediated protection against ALK inhibitors (*10*).

To study the eco-evolutionary dynamics of this interplay, we interrogated the competition between treatment naive H3122 cells and a derivative cell line in which we developed alectinib – a highly effective clinical ALK TKI (*11*) – resistance by selection in progressively increasing concentrations of the drug (*12*). We aimed to come to a quantitative understanding of how these dynamics were affected by clinically relevant concentrations of alectinib (0.5μM; see (*13*)) in the presence or absence of CAFs. To achieve this, we developed a novel assay for quantifying eco-evolutionary dynamics that is of independent interest to the general study of microscopic systems.

Mono vs mixed cultures & cost of resistance

To establish baseline characteristics, we performed assays in monotypic cultures of parental (alectinib-sensitive) and resistant cell lines with and without alectinib and CAFs. To determine the growth rate, which we use as a proxy for fitness, we grew parental and resistant cells in a time lapse microscope system (see Supplementary Methods for details). From the time series data, we inferred the growth rate of each cell type from 6 experimental replicates of each experimental condition, as seen in Figure 1. As expected, alectinib inhibited growth rates of parental cells, whereas the growth rate of the resistant cells was not affected. And as previously reported (*10*), we observed stromal protection against ALK TKI: CAFs provided a more significant growth advantage in the presence of alectinib.

If we limited ourselves to these monotypic assays then our observations would be consistent with the classic model of resistance which holds that in the absence of treatment (DMSO or DMSO + CAF) the resistant phenotype is neutral or even carries some inherent cost. For example, the experimental community assumes that the resistance granting mutation might have absolutely no effect in the absence of drug, and the modeling community considers explicit costs like the up-regulating pumps to remove the drug, investing in other defensive strate-

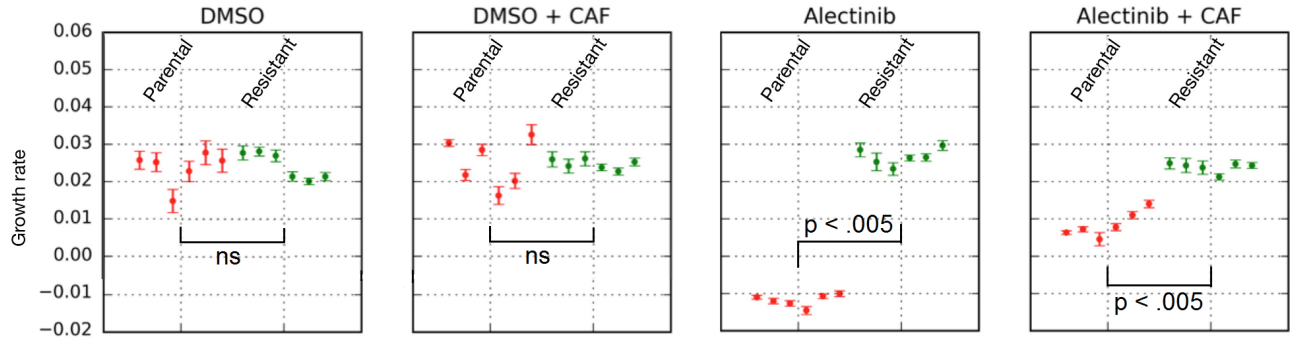

Figure 1: Monotypic culture growth rates for parental (red) and resistant (green) cells in indicated experimental conditions. Comparisons are made using Wilcoxon rank-sum.

gies, or lowering growth rate by switching to sub-optimal growth pathways (*3*, *14*). Finally, in the presence of drug, according to the classic model of resistance, resistance provides a relative benefit from increased survival or drug tolerance which – for modelers – offsets the cost.

Due to our interest in non-cell-autonomous biological interactions in cancer (*15*), we did not stop at monotypic assays. We continued our experiments over a range of initial proportions of resistant and parental cells for each of the four experimental conditions tested in monotypic culture. Other microscopic experimental systems in which frequency dependent fitness has been considered include, but are not limited to: *Escherichia coli* (*16*, *17*), yeast (*18*, *19*), bacterial symbionts of hydra (*20*), breast cancer (*15*) and pancreatic cancer (*21*); though none has been designed to measure evolutionary games directly. We used time lapse microscopy to follow the expansion of therapy resistant and parental cells, differentially labeled with stable expression of selectively neutral GFP and mCherry fluorescent proteins, respectively.

While the results of the monotypic culture matched expectations, we made a number of non-intuitive observations in our co-culture experiments. Figure 2 shows the resulting growth rates of each cell type in the co-culture experiments for all experimental (color, shape) and initial conditions (opacity is parental cell proportion). In the co-culture – unlike the monoculture – CAFs slightly improved the growth rates of the parental cells even in DMSO. More strikingly, even in the absence of drug, resistant cells tend to have a higher growth rate than parental cells. This is evident from most points being above the dotted diagonal line corresponding to equal growth rate of the sub-populations ($y = x$). The higher fitness of resistant cells we observe in the absence of drug throws in question the classic model of resistance.

Frequency dependence in fitness functions

Frequency dependence of both the parental and resistant growth rates is hinted at in Figure 2 where we see an increase in fitness of both cell types as the initial proportion of parental cells – represented by the opacity of each point – increases. This is shown more clearly in Figure 3. In all four conditions, we see that the growth rate of the resistant and parental cell lines depends linearly on the initial proportion of parental cells. In three of the conditions, the resistant cell growth rates increase with increased seeding proportion of parental cells, while the parental growth rates remain relatively constant (in the case of no CAFs) or slightly increasing (in the case of alectinib + CAFs). For example, in DMSO, this suggests that parental cells' fitness is independent of resistant cells: $w_P^{\text{DMSO}} = 0.025$. [1] However, resistant cells in monotypic culture have approximately the same fitness as parental cells (Figure 2a), but they benefit from the parental cells in co-culture: $w_R^{\text{DMSO}} = 0.025 + 0.015p$ (where p is the proportion of parental cells). [2] This suggests commensalism between resistant and parental cells, i.e. resistant cells benefit from the interaction with the parental cells, without exerting positive or negative impact on them.

The DMSO + CAF case differs from the other three in that we see a constant growth rate in resistant cells, but a linearly decreasing (in p) growth rate of parental cells: $w_P^{\text{DMSO + CAF}} = 0.025 + 0.01(1 - p)$.[3] This could be interpreted as CAFs switching the direction of commensalism between parental and resistant cells. Further, the stable co-existence enabled by the cross in fitness functions calls into question a widely held assumption that pre-existent resistance is a cell-autonomous binary switch to higher fitness (*22*).

Leader and Deadlock games in NSCLC

The tools of evolutionary game theory (EGT) are well suited for making sense of such frequency-dependent fitness (*21*, *23*–*29*). EGT defines a game as the rules mapping the population's strategy distribution to the fitness of individual strategies. Experimental EGT has used this to compare – usually qualitatively – the results of experiments to numeric simulations or analytic dynamics of specific games. Previous work has considered games like snowdrift (*19*), stag hunt (*20*), rock-paper-scissors (*16*), and public goods (*18*, *21*). We unite these parallel tracks by treating the game as an assayable hidden variable of a population and its environment.

[1] The actual line of best fit is $\hat{w}_P^{\text{DMSO}} = 0.025 - 0.001p$. This empirical fit has uncertainty, and w_P^{DMSO} is within the error-bars of $\hat{w}_P^{\text{DMSO}}$.

[2] The empirical line of best fit is $\hat{w}_R^{\text{DMSO}} = 0.027 + 0.013p$. But w_R^{DMSO} is within error of $\hat{w}_R^{\text{DMSO}}$.

[3] The empirical line of best fit is $\hat{w}_P^{\text{DMSO + CAF}} = 0.035 - 0.009p$. But $w_P^{\text{DMSO + CAF}}$ is within error of $\hat{w}_P^{\text{DMSO + CAF}}$.

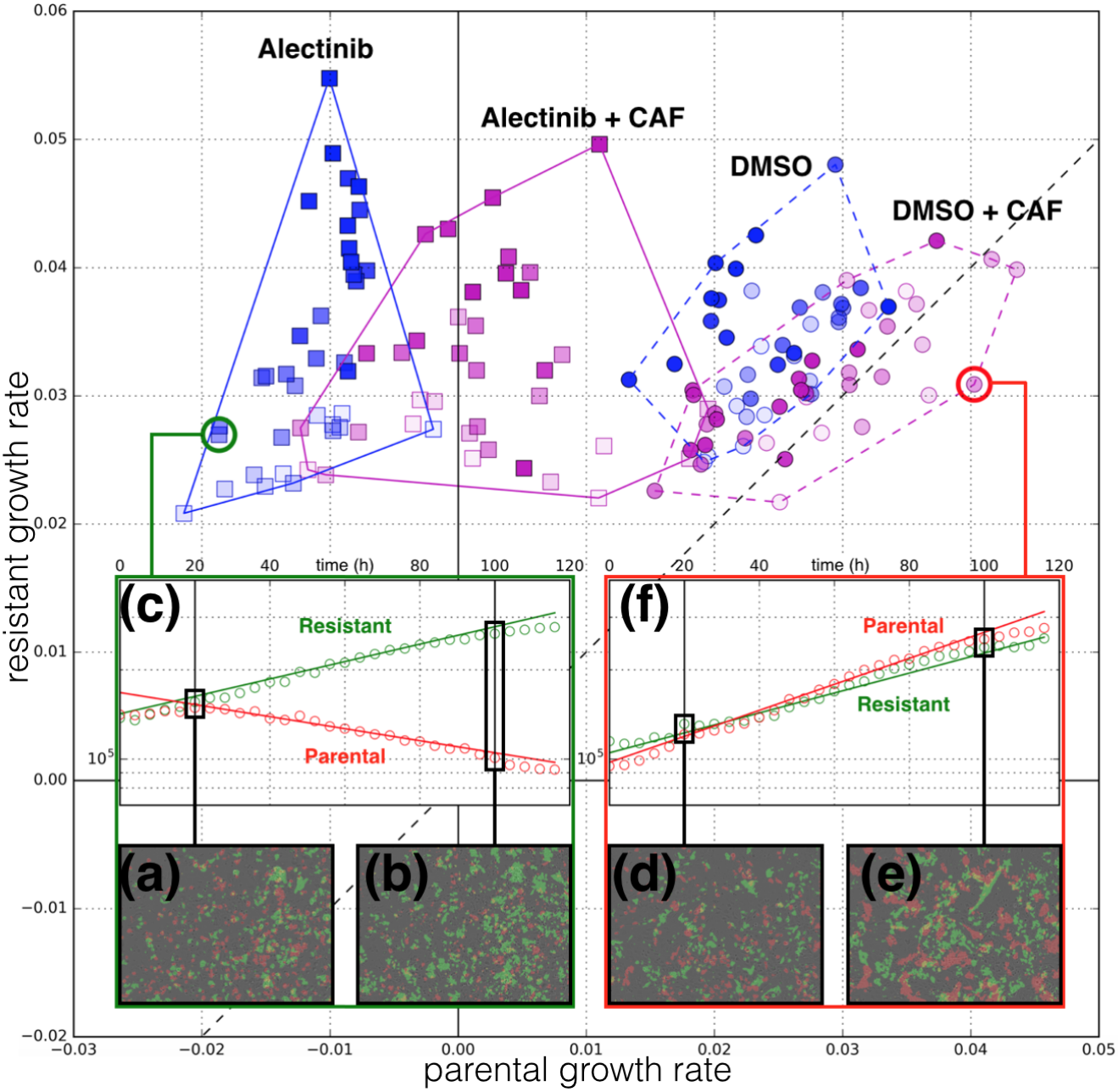

Figure 2: Coculture growth rates across four experimental conditions. Each point in the main figure is a separate well with initial proportion of parental cells represented by opacity and experimental condition represented by shape (DMSO: circle; Alectinib; square) and colour (no CAF: blue; + CAF: magenta). Each well's x-position corresponds to parental growth rate and y-position for resistant growth rate; dotted block line corresponds to the line of equal fitness at $x = y$. **(a,b,d,e)** In each well, we quantify population size by fluorescent area of each cell type from 30 time-lapse microscopy images. **(c,f)**: time-series of parental and resistant population size for two example wells. Inset x-axis is time, y-axis is log of population size. Median growth rate and confidence intervals (omitted) were estimated for each well using the Theil-Sen estimator, and serve as the coordinates in the main figure. See Figure 3 for growth rate confidence intervals.

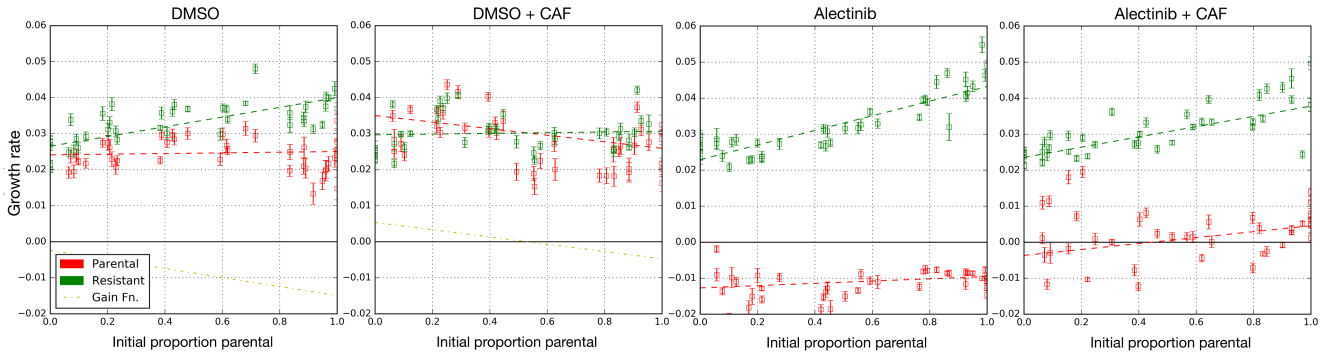

Figure 3: Fitness functions for competition of parental vs. resistant NSCLC. For each plot: growth rate with confidence intervals versus initial proportion of parental cells. Red data points are growth rates of parental cells, and green for resistant cells. Dotted lines represent the linear fitness function of best fit, and the yellow dotted line is the gain function for parental (see Figure 4a); fit error visualised in Figure 4b.

To measure the game that describes these interactions, it is important to focus on the gain function (see (*29*, *30*) for a theoretical perspective): the increase in growth rate that a hypothetical player would get in 'switching' from being parental to resistant with all other variables held constant. In other words, we need to look at how the difference between resistant and parental growth rates varies with initial proportion of parental cells. The relatively good fit of a linear dependence of growth rates on parental seeding proportion allows us to model the interaction as a matrix game – a well-studied class of evolutionary games (see model in Figure 4a). Note that this linearity is not guaranteed for arbitrary experimental systems. For example, the game between the two Betaproteobacteria *Curvibacter* sp. AEP1.3 and *Duganella* sp. C1.2 was described by a quadratic gain function (*20*). Future work can extend our assay to non-matrix games.

Two strategy matrix games have a convenient representation in a two dimensional game-space and can produce all possible linear gain functions. More importantly, from a linear gain function, it is possible to infer the corresponding matrix game, up-to constant offsets on each column. Since the game type and resultant dynamics are invariant under constant offsets to the columns, this means we can infer the game played by the cancer cells (see the model in Figure 4a for details). This is the output of our game assay. We plot the inferred games in a game-space spanned by the theoretical fitness advantage a single resistant invader would have if introduced into a parental monotypic culture versus the fitness advantage of a parental invader in a resistant monotypic culture; as shown in Figure 4b. In this representation, there are four qualitatively different types of games corresponding to the four quadrants with an illustrative dynamic flow inset in the corner of each quadrant. We can see that the game corresponding to DMSO + CAF – although quantitatively similar to DMSO – is of a qualitatively different type compared to all three of the other combinations.

We can also convert our inferred fitness functions from Figure 3 into a payoff matrix. We do this by having each row correspond to a strategy's fitness function with the column entries as the $p = 1$ and $p = 0$ intersects of this line of best fit. If we look at our empirical measurements for DMSO + CAF (upper-right quadrant Figure 4b) we see the Leader game, and Deadlock in the other three cases. To our knowledge, neither of these games is considered in the prior theoretical EGT literature in oncology. In addition to adding two new entries to the catalogue of games that cancers play, our results also support existing theoretical work in mathematical oncology that considers treatment (or other environmental differences) as changes between qualitatively different game regimes (*26*–*29*). In this framework, treatment has the goal not to directly target the cells, but instead perturb the game they are playing and allow evolution to drive unwanted cancer subclones to extinction through competition. Before this study, this possibility has been largely taken as a theoretical postulate. In our system, we can view an untreated tumour as similar to DMSO + CAF and thus following the Leader game. Treating with alectinib (move to Alectinib + CAF) or eliminating CAFs through a stromal directed therapy (move to DMSO), moves the game into the lower-right quadrant of Figure 4b, and the game becomes a Deadlock game. This switch allows us to show that this theoretical construct of EGT – that treatment can qualitative change the type of game – has an experimental implementation.

A particularly important difference between Leader and Deadlock dynamics is the existence of an internal fixed point in Leader but not in Deadlock. We can see convergence towards this fixed point in the DMSO + CAF condition of Figure 4c, and no such convergence in the other three cases (Figure 4d for Alectinib + CAF; Supplementary Figure 5). Since the DMSO + CAF condition is our closest to an untreated patient, it has important consequences for latent resistance. Classical models of resistance assume a rare or *de novo* mutant taking over the population after the introduction of drug. In our experimental system, however, it is possible for negative frequency dependent selection to push the population towards a stable polyclonal tumour of resistant and sensitive cells before the introduction of drug. This allows for much higher levels of pre-existing heterogeneity in resistance than predicted by the classical picture.With this pre-existing heterogeneity, tumour resistance can emerge faster and more robustly; helping us to better understand why all patients eventually develop resistance to targeted therapies like alectinib.

$$\begin{array}{cc} & \begin{matrix} P & R \end{matrix} \\ \begin{matrix} P \\ R \end{matrix} & \begin{pmatrix} A & B \\ C & D \end{pmatrix} \end{array} \Rightarrow \begin{cases} \frac{d}{dt}N_P = N_P \overbrace{\left(A\frac{N_P}{N_P+N_R} + B\frac{N_R}{N_P+N_R}\right)}^{w_P\text{: parental growth rate}} \\ \frac{d}{dt}N_R = N_R \underbrace{\left(C\frac{N_P}{N_P+N_R} + D\frac{N_R}{N_P+N_R}\right)}_{w_R\text{: resistant growth rate}} \end{cases}$$

$$\Rightarrow \frac{dp}{dt} = p(1-p)\overbrace{\left(\underbrace{(B-D)}_{\substack{\text{relative fitness of} \\ \text{parental invader}}}(1-p) - \underbrace{(C-A)}_{\substack{\text{relative fitness of} \\ \text{resistant invader}}}p\right)}^{\text{gain function for } p}$$

$$\text{where } p = \frac{N_P}{N_P+N_R}.$$

(a) Replicator dynamics for parental-resistant NSCLC.

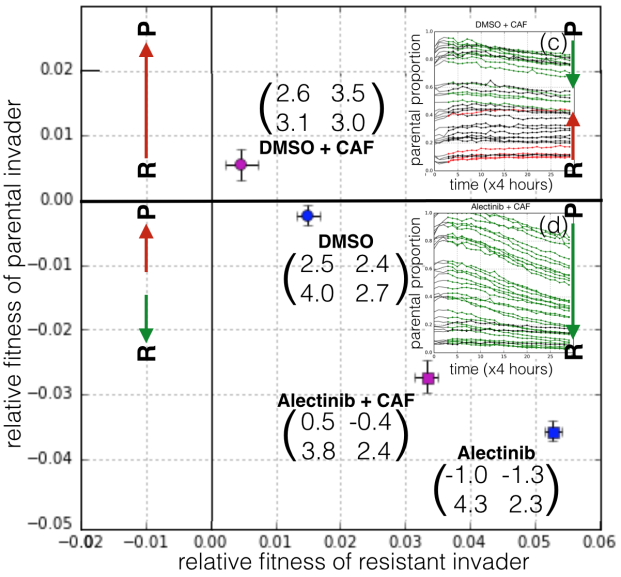

(b) Two dimensional game space.

Figure 4: Measured games. (a) Consider two strategies in a cancer cell co-culture: parental (P) and resistant (R). When subpopulation of P interacts with P then each experience a fitness effect A; when P encounters R then P experience fitness effect B and R fitness effect C; two Rs interaction experience fitness effects D. This is summarised in the matrix above, where the focal agent selects row and alter selects column; the matrix entry is then the fitness effect for the focal. This can be translated into a simple exponential growth model for the number of parental N_P and number of resistant N_R cells. The dynamics of the proportion of parental cells $p = \frac{N_P}{N_P+N_R}$ over time is described by the replicator equation (bottom). Notice that for a matrix game, the gain function can be an arbitrary linear function of p. **(b)** We plot the four games measured in vitro. The x-axis is the relative fitness of a resistant focal in a parental monotypic culture: $C-A$. The y-axis is the relative fitness of a parental focal in a resistant monotypic culture: $B-D$. Games measured in our experimental system are given as specific points with error bars based on goodness of fit of linear fitness functions in Figure 3. The games corresponding to our conditions are given as matrices (with entries multiplied by a factor of 100) by their label. The game space is composed of four possible dynamical regimes, one for each quadrant. The typical dynamics of each dynamic regime are represented as qualitative flow diagram between parental (P) and resistant (R) strategies: an upward red arrow corresponds to an increase in the parental subpopulation, and a downward green arrow correspond to an increase in the green subpopulation. In the case of the two dynamic regimes observed in our NSCLC system, **(c,d)** inset shows the experimental time-series of proportion of parental cells for DMSO + CAF (c) and Alectinib + CAF (d). Each line corresponds to the time dynamics of a separate well. A line is coloured green if proportion of resistant cells increased from start to end; red if proportion of parental cells increased; black if statistically indistinguishable proportions at start and end. Inset x-axis is time, and y-axis is proportion of parental cells as measured from time-lapse microscopy. See Supplementary Figure 5 for proportion dynamics of all four games. See Supplementary Figure 6 for density dynamics and their correspondence to the exponential growth model from Figure 4a.

Conclusion

Drug-sensitive (parental) and resistant cells interact not only with alectinib, but also with each other and microenvironmental factors like CAFs. We showed that the relative fitness advantage of resistant over parental cells – the gain function characterizing replicator dynamics – is a linear function of the initial proportion of sensitive cells. Surprisingly, resistant cells have an advantage over parental cells even in DMSO, throwing into question the common theoretical postulate that resistance is neutral or comes at a cost. Measuring the gain function has enabled us to develop an assay that represents the inter-dependence between parental and resistant cells as a matrix game. Not only are these games quantitatively different among the four environmental conditions – see Figure 4b – but they are also of two qualitatively different types: a Leader game in the case of DMSO + CAF and Deadlock in the other three cases.

This ability of treatment to qualitative change the type of game being played provides the first empirical demonstration of the principal "don't treat the player, treat the game." Our hope is that this empirical connection allows for potential translations of existing oncologic EGT literature to the clinic. Unfortunately, the Leader and Deadlock games are understudied in mathematical oncology, and we hope that our observation of them will motivate theorists to explore them in more detail. One difference between these game types is already clear: in the case of Leader there is negative frequency dependence selection toward a coexistence of parental and resistant cells – which we confirm for DMSO + CAF in Figure 4c – while for Deadlock there is selection towards a completely resistant tumour. Since DMSO + CAF is the closest analogue to a pre-treatment patient in our *in vitro* system, this suggests that there might be much higher levels of initial heterogeneity in drug resistance than prior theory would suggest and throws into question the concept of rare pre-existing resistant clones. If this result holds *in vivo* and/or for other cancers it will help explain the ubiquity and speed of resistance that undermines our abilities to cure patients or control their disease. Building a catalogue of the games cancers play – by adopting our game assay in other cancers, and other experimental contexts – can help resolve this and others questions, and serve as foundation for a new strategy in cancer therapy: treating the game.

Acknowledgements

JGS would like to acknowledge the NIH Loan Repayment program for their generous support of his research in general as well as Miles for Moffitt for generously supporting this work. We would also like to thank Mohamed Abazeed, Peter Jeavons, and Konstantine Kaznatcheev for helpful discussions.

References

1. L. M. Merlo, J. W. Pepper, B. J. Reid, C. C. Maley, *Nature Reviews Cancer* **6**, 924–935 (2006).
2. G. H. Heppner, *Cancer Research* **44**, 2259–2265 (1984).
3. A. Ibrahim-Hashim *et al.*, *Cancer Research*, 2844 (2017).
4. J. Scott, A. Marusyk, *Biochimica et Biophysica Acta: Reviews on Cancer* (2017).
5. A. T. Shaw *et al.*, *New England Journal of Medicine* **368**, 2385–2394 (2013).
6. A. T. Shaw, J. A. Engelman, *Journal of Clinical Oncology* **31**, 1105–1111 (2013).
7. R. J. Gillies, D. Verduzco, R. A. Gatenby, *Nature Reviews Cancer* **12**, 487–493 (2012).
8. R. Katayama, C. M. Lovly, A. T. Shaw, *Clinical Cancer Research* **21**, 2227–2235 (10 2015).
9. A. Marusyk *et al.*, *Cancer Research* **76**, 6495–6506 (2016).
10. T. Yamada *et al.*, *Clinical Cancer Research* **18**, 3592–3602 (2012).
11. S.-H. I. Ou *et al.*, *Journal of Clinical Oncology* **34**, 661–668 (2015).
12. A. Dhawan *et al.*, *Scientific Reports* **7** (2017).
13. T. Seto *et al.*, *The Lancet Oncology* **14**, 590–598 (2013).
14. A. R. Anderson, A. M. Weaver, P. T. Cummings, V. Quaranta, *Cell* **127**, 905–915 (2006).
15. A. Marusyk *et al.*, *Nature* **514**, 54 (2014).
16. B. Kerr, M. A. Riley, M. W. Feldman, B. J. Bohannan, *Nature* **418**, 171–174 (2002).
17. R. Maddamsetti, R. E. Lenski, J. E. Barrick, *Genetics* **200**, 619–631 (2015).
18. R. C. MacLean, I. Gudelj, *Nature* **441**, 498 (2006).
19. J. Gore, H. Youk, A. Van Oudenaarden, *Nature* **459**, 253–256 (2009).
20. X.-Y. Li *et al.*, *Journal of The Royal Society Interface* **12**, 20150121 (2015).
21. M. Archetti, D. A. Ferraro, G. Christofori, *Proceedings of the National Academy of Sciences* **112**, 1833–1838 (2015).
22. L. A. Diaz Jr *et al.*, *Nature* **486**, 537 (2012).
23. J Maynard Smith, G. R. Price, *Nature* **246**, 15 (1973).
24. I. P. Tomlinson, W. F. Bodmer, *British Journal of Cancer* **75**, 157–160 (1997).
25. I. P. Tomlinson, *European Journal of Cancer* **33**, 1495–1500 (1997).
26. D. Basanta *et al.*, *British Journal of Cancer* **106**, 174–181 (2012).
27. M. Archetti, *British Journal of Cancer* **109**, 1056–1062 (2013).
28. A. Kaznatcheev, J. G. Scott, D. Basanta, *Journal of The Royal Society Interface* **12**, 20150154 (2015).
29. A. Kaznatcheev, R. Vander Velde, J. G. Scott, D. Basanta, *British Journal of Cancer* (2017).
30. J. Peña, L. Lehmann, G. Nöldeke, *Journal of Theoretical Biology* **346**, 23–33 (2014).
31. M. Mediavilla-Varela, K. Boateng, D. Noyes, S. J. Antonia, *BMC Cancer* **16**, 176 (2016).